

## 14: A high pitch angle structure in the Sagittarius Arm

[M. A. Kuhn](#) (1), [R. A. Benjamin](#) (2), [C. Zucker](#) (3), [A. Krone-Martins](#) (4,5), [R. S. de Souza](#) (6), [A. Castro-Ginard](#) (7), [E. E. O. Ishida](#) (8,9), [M. S. Povich](#) (10), [L. A. Hillenbrand](#) (1),

Context: In spiral galaxies, star formation tends to trace features of the spiral pattern, including arms, spurs, feathers, and branches. However, in our own Milky Way, it has been challenging to connect individual star-forming regions to their larger Galactic environment owing to our perspective from within the disk. One feature in nearly all modern models of the Milky Way is the Sagittarius Arm, located inward of the Sun with a pitch angle of  $\sim 12$  deg.

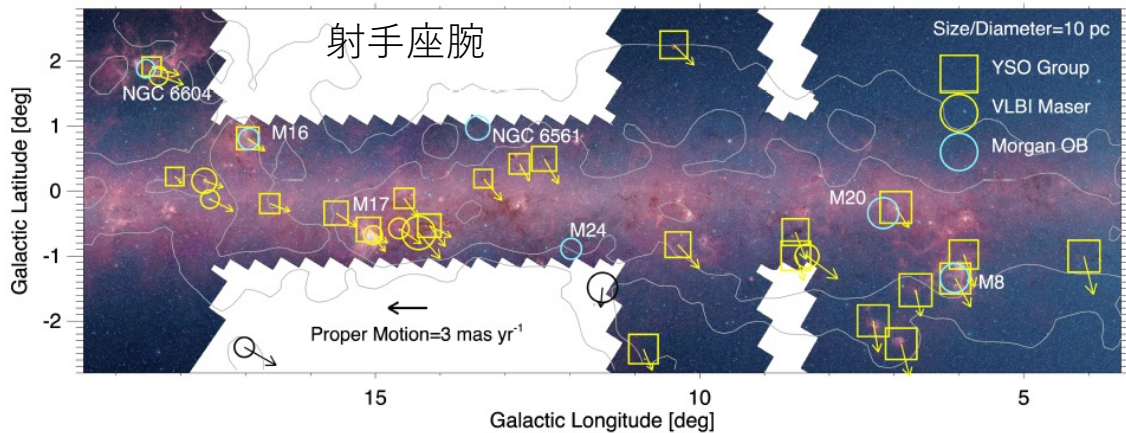
Aims: We map the 3D locations and velocities of star-forming regions in a segment of the Sagittarius Arm using young stellar objects (YSOs) from the Spitzer/IRAC Candidate YSO (SPICY) catalog to compare their distribution to models of the arm.

Methods: Distances and velocities for these objects are derived from Gaia EDR3 astrometry and molecular line surveys. We infer parallaxes and proper motions for spatially clustered groups of YSOs and estimate their radial velocities from the velocities of spatially associated molecular clouds.

Results: We identify 25 star-forming regions in the Galactic longitude range  $l \sim 4.0$ - $18.5$  deg arranged in a narrow,  $\sim 1$  kpc long linear structure with a high pitch angle of  $\psi = 56$  deg and a high aspect ratio of  $\sim 7:1$ . This structure includes massive star-forming regions such as M8, M16, M17, and M20. The motions in the structure are remarkably coherent, with velocities in the direction of Galactic rotation of  $|V_\phi| = 240 \pm 3$  km/s (slightly higher than average) and slight drifts toward the Galactic center ( $-4.3$  km/s) and in the negative Z direction ( $V_z \sim -2.9$  km/s). The rotational shear experienced by the structure is  $\Delta\Omega = 4.6$  km/s/kpc.

Conclusions: The observed 56 deg pitch angle is remarkably high for a segment of the Sagittarius Arm. We discuss possible interpretations of this feature as a substructure within the lower pitch angle Sagittarius Arm, as a spur, or as an isolated structure.

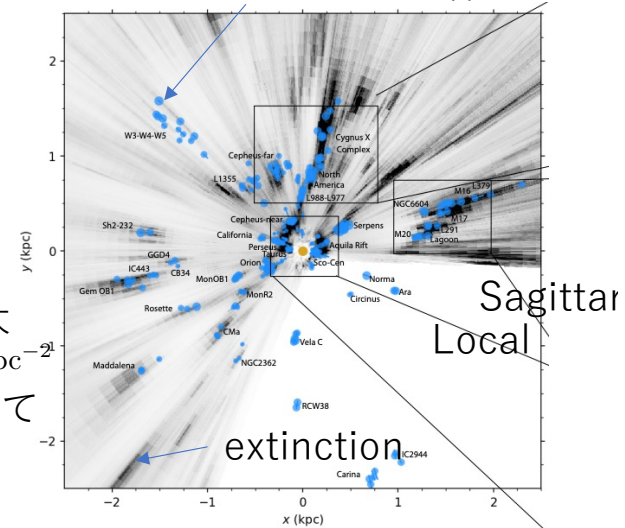
spiral armの中にspurs (luminous stellar features),  
feathers (dust features), branches



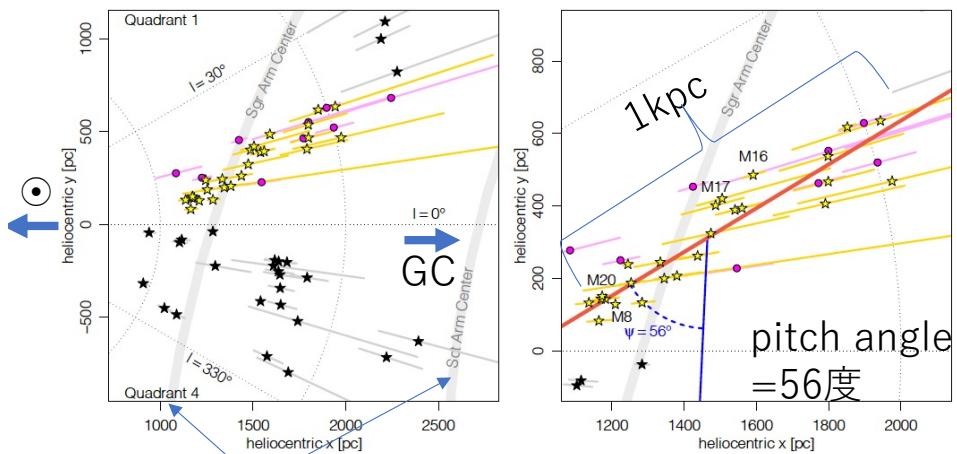
1次元構造  
長さ950pc  
軸比=14:2:1  
ピッチ角=56°  
システムテック  
な構造

射手座腕より大  
 $S_{24\mu\text{m}} \sim 5 \times 10^{40} \text{ erg s}^{-1} \text{ kpc}^{-2}$   
 予想HII knotsとして  
 中間クラス

Star Formation  
Handbook天体



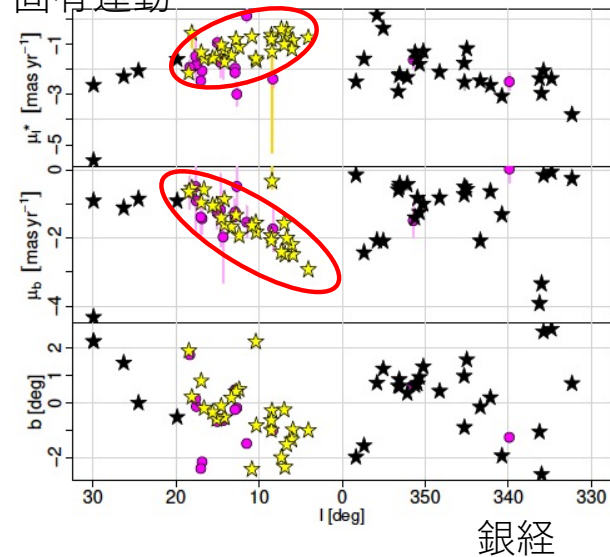
Gaia位置天文



大局的な腕

★☆☆YSO,●maser

## 固有運動



cf. Zucker+2020

$$|V_\phi| \sim 240 \pm 3 \text{ km s}^{-1}$$

$$|V_B| = -4.3 \pm 3.5 \text{ km s}^{-1}$$

$$|V_z| = -2.9 \text{ km s}^{-1}$$

$$\text{shear} = 4.6 \text{ km s}^{-1} \text{ kpc}$$

$$\tau_{sh} \sim 90 \text{ Myr}$$

Wada,Koda2004

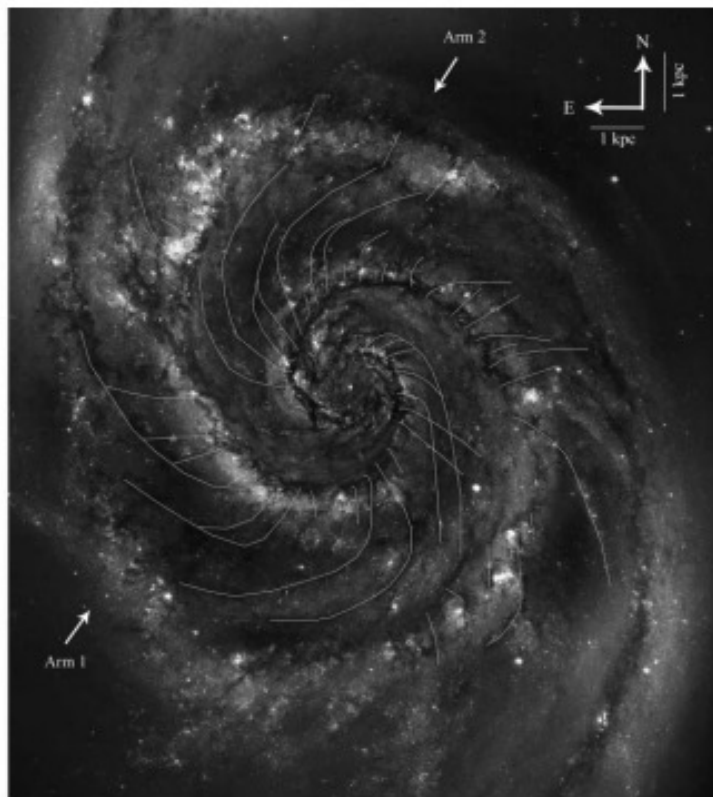


FIG. 1.—Prototypical galaxy with feathers: NGC 5194. Feathers are marked by white lines. (See the electronic version for the full-resolution image of this figure and all other figures.)

La Vigne, Vogel, Ostriker 2006

成因？重力、速度シア、銀河衝撃波、MHD

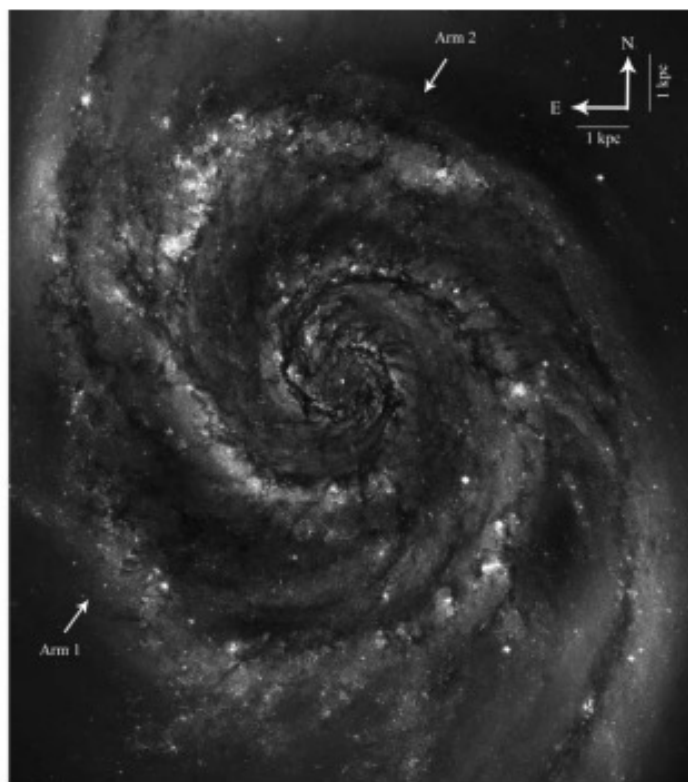
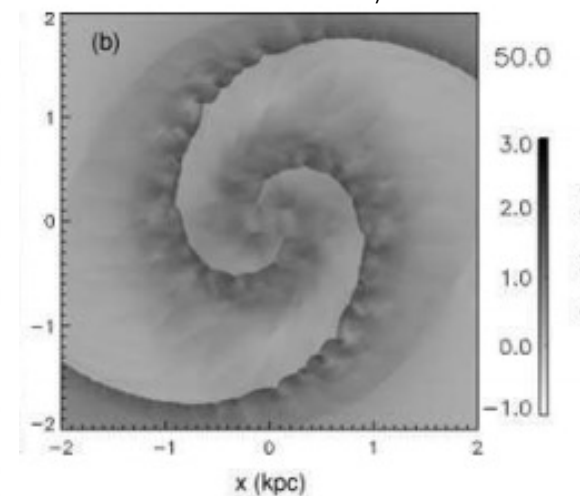
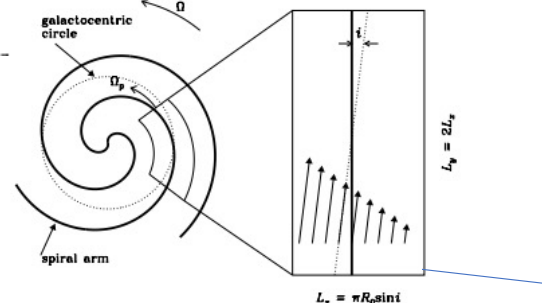
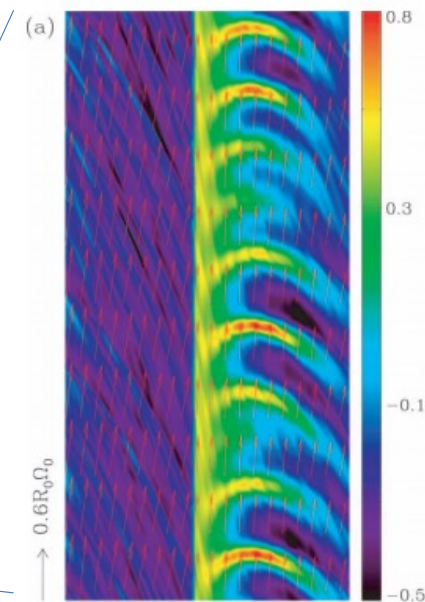


FIG. 3.—NGC 5194, with the feather overlay omitted.



Kim,Ostriker 2002



## 15: The density structure of supersonic self-gravitating turbulence

[Shivan Khullar](#), [Christoph Federrath](#), [Mark R. Krumholz](#), [Christopher D. Matzner](#)

We conduct numerical experiments to determine the density probability distribution function (PDF) produced in supersonic, isothermal, self-gravitating turbulence of the sort that is ubiquitous in star-forming molecular clouds. Our experiments cover a wide range of turbulent Mach number and virial parameter, allowing us for the first time to determine how the PDF responds as these parameters vary, and we introduce a new diagnostic, the dimensionless star formation efficiency versus density ( $\epsilon_{\text{ff}}(s)$ ) curve, which provides a sensitive diagnostic of the PDF shape and dynamics. We show that the PDF follows a universal functional form consisting of a log-normal at low density with two distinct power law tails at higher density; the first of these represents the onset of self-gravitation, and the second reflects the onset of rotational support. Once the star formation efficiency reaches a few percent, the PDF becomes statistically steady, with no evidence for secular time-evolution at star formation efficiencies from about five to 20 percent. We show that both the Mach number and the virial parameter influence the characteristic densities at which the log-normal gives way to the first power-law, and the first to the second, and we extend (for the former) and develop (for the latter) simple theoretical models for the relationship between these density thresholds and the global properties of the turbulent medium.

磁場なし、等温、3次元の駆動乱流、  
density PDF (probability distribution  
function)

- (1) 対数正規分布
- (2) 指数分布1
- (3) 指数分布2

基礎方程式

$$\left[ \begin{array}{l} \frac{\partial \rho}{\partial t} + \nabla \cdot (\rho \mathbf{v}) = 0, \\ \rho \frac{\partial \mathbf{v}}{\partial t} + \rho (\mathbf{v} \cdot \nabla) \mathbf{v} = -\rho (\mathbf{g} + \mathbf{F}_{\text{turb}}) - \nabla (P_{\text{th}}), \\ \mathbf{g} = -\nabla \phi_{\text{gas}} + \mathbf{g}_{\text{sink}}, \\ \nabla^2 \phi_{\text{gas}} = 4\pi G \rho, \end{array} \right.$$

FLASH

$$\left[ \begin{array}{l} \mathcal{M} = \sigma_V / c_s \\ \alpha_{\text{vir},0} = \frac{5\sigma_V^2 L}{6GM_c} \end{array} \right.$$

solenoidal+compressibleの  
natural mixture Federrath2010

LN+PN  $s = \log \rho$

$$p(s) = \begin{cases} \frac{N}{\sqrt{2\pi}\sigma_s^2} \exp\left[-\frac{(s-s_0)^2}{2\sigma_s^2}\right] & s < s_g, \\ Np_0 e^{-s\alpha_g} & s \geq s_g, \end{cases}$$

正規分布  
対数分布

独立パラメータ2個  $\alpha_g, \sigma_s$

LN+2PN

$$p(s) = \begin{cases} \frac{N}{\sqrt{2\pi}\sigma_s^2} \exp\left[-\frac{(s-s_0)^2}{2\sigma_s^2}\right] & s < s_g, \\ Np_0 \exp(-s\alpha_g) & s_g \leq s \leq s_d, \\ Np_1 \exp(-s\alpha_d) & s_d \leq s \leq s_{\text{sink}}, \end{cases}$$

独立パラメータ4個  $\alpha_g, \sigma_s, \alpha_d, s_d$

Star Formation Efficiency

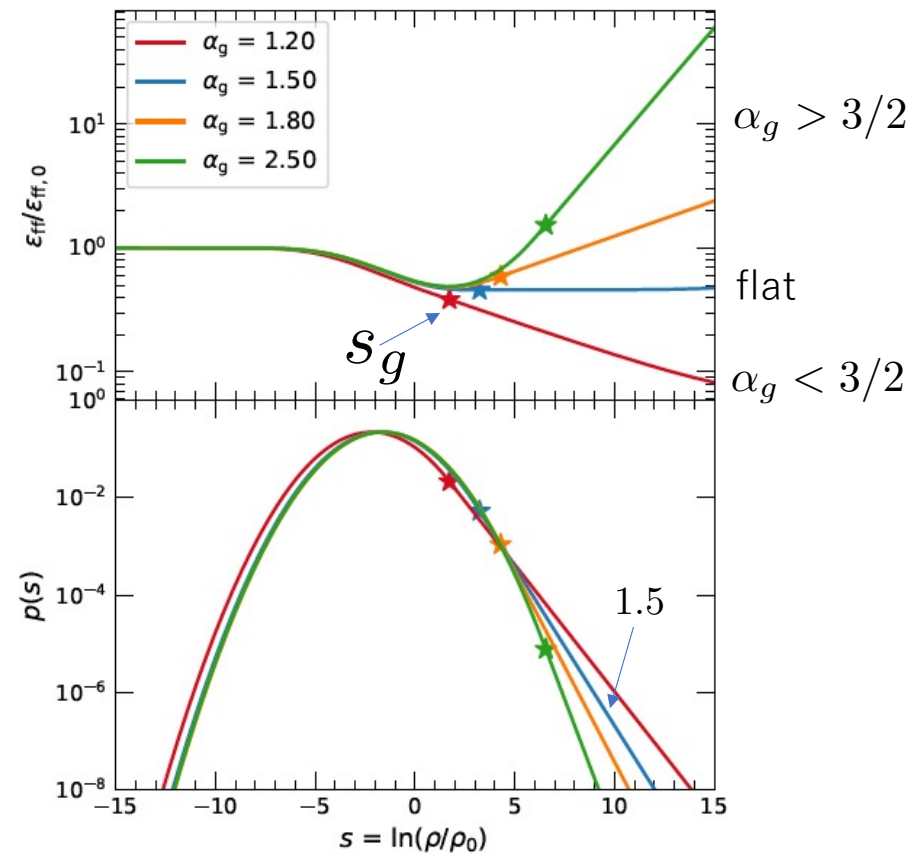
$$\epsilon_{\text{ff}} = \frac{\text{SFR}}{M_{\text{gas}}/t_{\text{ff}}}$$



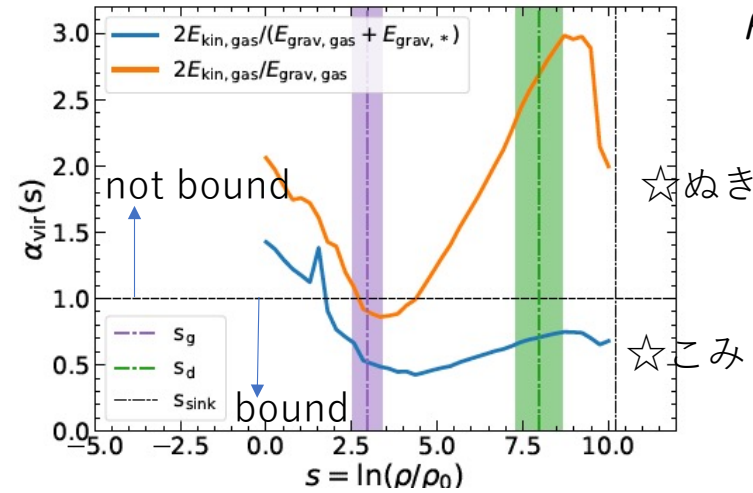
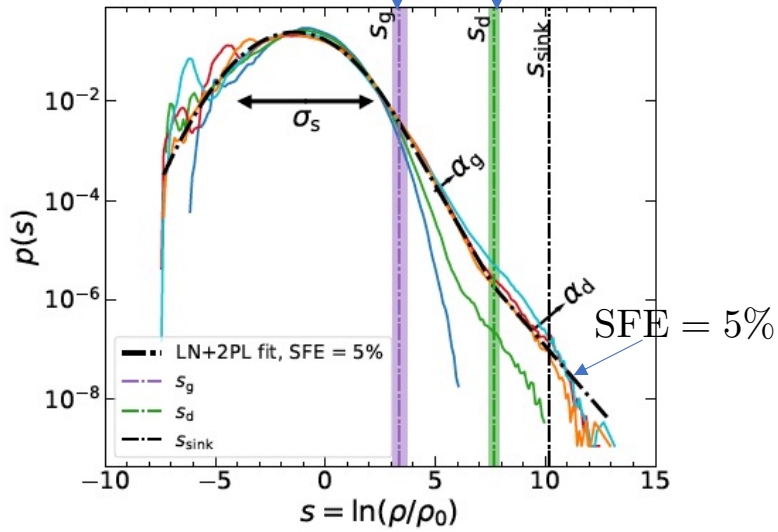
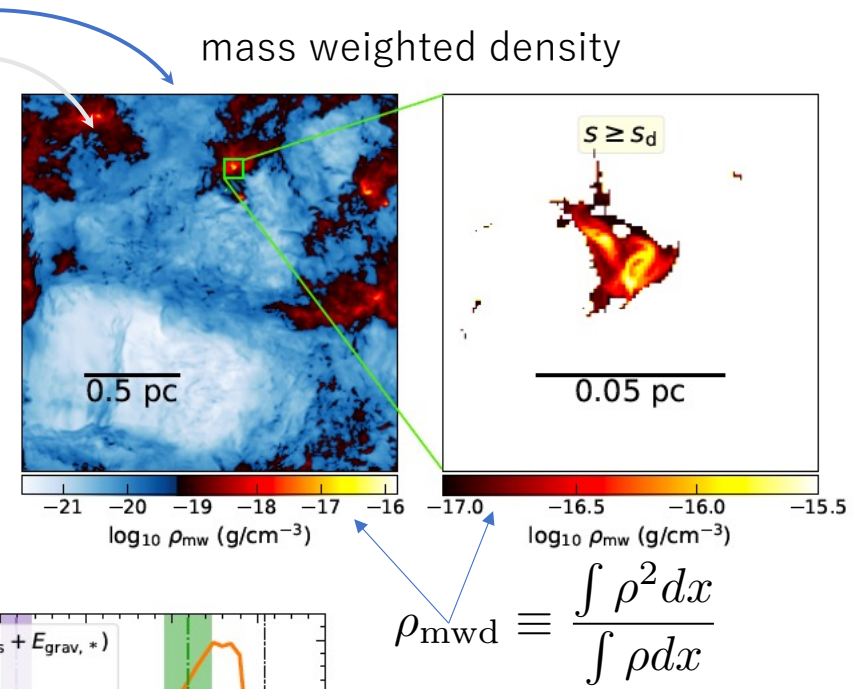
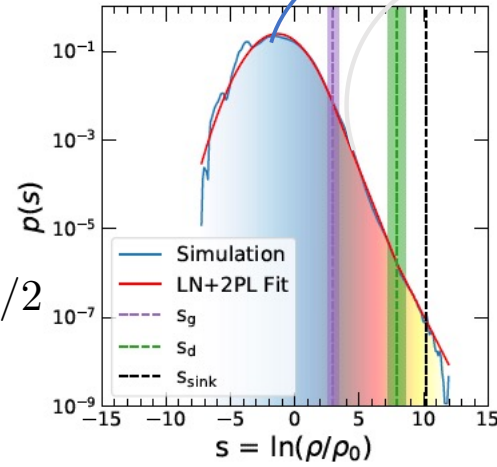
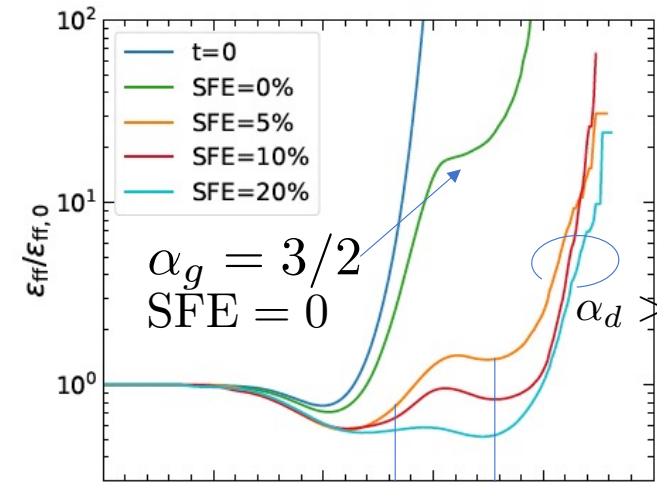
$$\epsilon_{\text{ff}}(s) = \frac{\text{SFR}}{M_{\text{gas}}(s)/t_{\text{ff}}(s)} = \frac{\text{SFR} \times t_{\text{ff},0}}{M_{\text{tot}}} \frac{\int_s^\infty e^{-s/2} p(s) ds}{\int_s^\infty p(s) ds \times \int_s^\infty e^s p(s) ds}, \propto e^{(-3/2+\alpha)s}$$

$s$ 以上の密度のガスの全質量

$s$ 以上の密度の平均自由落下時間



$$\mathcal{M} = 5 \quad \alpha_{\text{vir},0} = 1$$



- 1) bound system @  $s_g$
- 2) rotation support scale

## 16: The Transition of Polarized Dust Thermal Emission from the Protostellar Envelope to the Disk Scale

[Ka Ho Lam](#) (1), [Che-Yu Chen](#) (1 and 2), [Zhi-Yun Li](#) (1), [Haifeng Yang](#) (3), [Erin G. Cox](#) (4), [Leslie W. Looney](#) (5), [Ian Stephens](#) (6 and 7)

Polarized dust continuum emission has been observed with ALMA in an increasing number of deeply embedded protostellar systems. It generally shows a sharp transition going from the protostellar envelope to the disk scale, with the polarization fraction typically dropping from  $\sim 5\%$  to  $\sim 1\%$  and the inferred magnetic field orientations becoming more aligned with the major axis of the system. We quantitatively investigate these observational trends using a sample of protostars in the Perseus molecular cloud and compare these features with a non-ideal MHD disk formation simulation. We find that the gas density increases faster than the magnetic field strength in the transition from the envelope to the disk scale, which makes it more difficult to magnetically align the grains on the disk scale. Specifically, to produce the observed  $\sim 1\%$  polarization at  $\sim 100\text{au}$  scale via grains aligned with the B-field, even relatively small grains of  $1\text{ }\mu\text{m}$  in size need to have their magnetic susceptibilities significantly enhanced (by a factor of  $\sim 20$ ) over the standard value, potentially through superparamagnetic inclusions. This requirement is more stringent for larger grains, with the enhancement factor increasing linearly with the grain size, reaching  $\sim 2 \times 10^4$  for millimeter-sized grains. Even if the required enhancement can be achieved, the resulting inferred magnetic field orientation in the simulation does not show a preference for the major axis, which is inconsistent with the observed pattern. We thus conclude that the observed trends are best described by the model where the polarization on the envelope scale is dominated by magnetically aligned grains and that on the disk scale by scattering.

磁気分極  $\mathbf{M} = \chi \mathbf{\Omega} / \gamma$

$\chi$ : magnetic susceptibility

磁気モーメント:  $|\mathbf{M}| 4\pi a^3/3 = |\mathbf{M}|V$

磁気トルク  $= |\mathbf{M}|VB$

ラーマー歳差時間:

$$t_L = \frac{2\pi I |\mathbf{\Omega}|}{|\mathbf{M}|VB} = \frac{4\pi(\rho_s V)a^2/5 \cdot \gamma}{\chi VB} = \left(\frac{4\pi\gamma}{5}\right) \frac{\rho_s a^2}{\chi B}$$

$$= 2.6 \times 10^{11} \text{ s}$$

$$\times \hat{\chi}^{-1} \left(\frac{\rho_s}{3 \text{ g/cm}^3}\right) \left(\frac{T_s}{15 \text{ K}}\right) \left(\frac{B}{5 \text{ mG}}\right)^{-1} \left(\frac{a}{1 \text{ mm}}\right)^2,$$

常磁性体

$$\hat{\chi} \sim 1$$

ガスダンピング時間

$$t_d = \frac{2\sqrt{\pi}}{5} \frac{\rho_s a}{n_g m_g v_{g,th}}$$

$$= 3.37 \times 10^8 \text{ s}$$

$$\times \left(\frac{\rho_s}{3 \text{ g/cm}^3}\right) \left(\frac{a}{1 \text{ mm}}\right) \left(\frac{n_g}{5 \times 10^9 \text{ cm}^{-3}}\right)^{-1} \left(\frac{T_g}{15 \text{ K}}\right)^{-1/2}$$

磁場に整列が起こるには  $t_L < t_d$

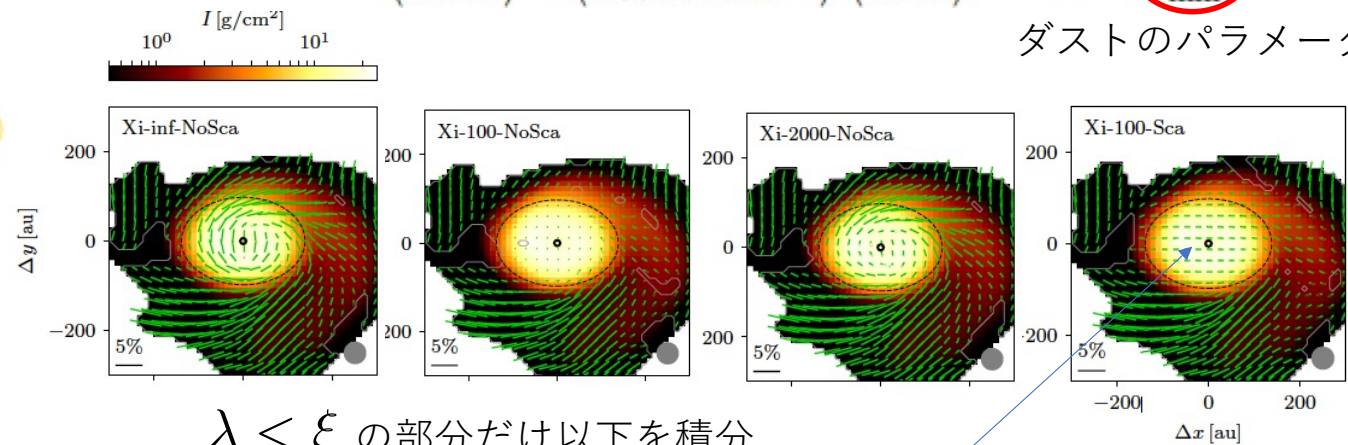
磁場整列の条件

$$\frac{t_L}{t_d} = 771 \times \left(\frac{a_{\text{mm}}}{\hat{\chi}}\right) \left(\frac{B}{5 \text{ mG}}\right)^{-1} \left(\frac{n_g}{5 \times 10^9 \text{ cm}^{-3}}\right) \left(\frac{T}{15 \text{ K}}\right)^{3/2} < \xi$$

$$\hat{\chi} \sim 1 \quad a < 1 \mu\text{m} \quad \text{サブミクロンダスト}$$

$$\lambda \equiv 771 \times \left(\frac{B}{5 \text{ mG}}\right)^{-1} \left(\frac{n_g}{5 \times 10^9 \text{ cm}^{-3}}\right) \left(\frac{T}{15 \text{ K}}\right)^{3/2} < \xi \equiv \frac{\hat{\chi}/\eta}{a_{\text{mm}}},$$

ダストのパラメータ



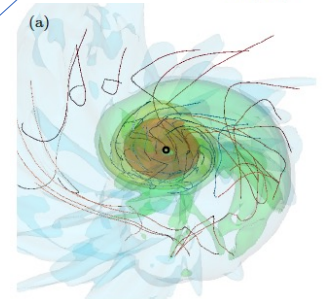
$\lambda < \xi$  の部分だけ以下を積分

$$I = \int \rho \left(1 - \alpha \left(\frac{\cos^2 \gamma}{2} - \frac{1}{3}\right)\right) ds,$$

$$Q = \alpha \int \rho \cos 2\psi \cos^2 \gamma ds,$$

$$U = \alpha \int \rho \sin 2\psi \cos^2 \gamma ds,$$

成り立たない部分に、  
短軸方向1%  
の散乱偏光



## 17: The link between gas and stars in the S254-S258 star-forming region

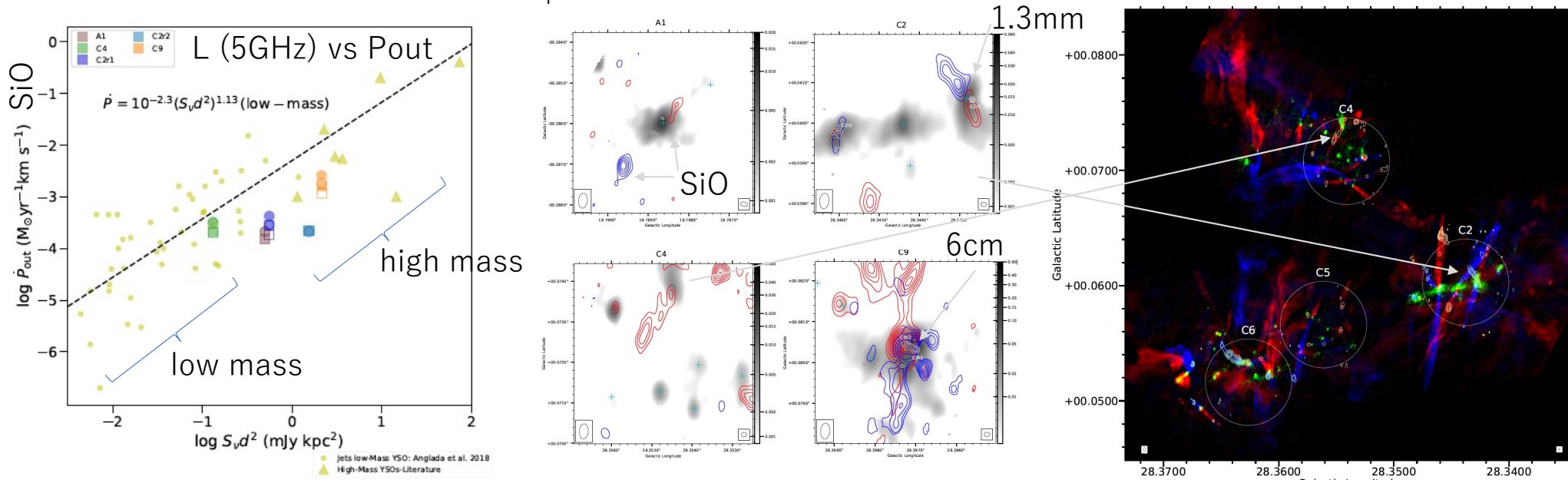
[D. A. Ladeyschikov](#), [M. S. Kirsanova](#), [A. M. Sobolev](#), [M. Thomasson](#), [V. Ossenkopf-Okada](#), [M. Juvela](#), [S. A. Khaibrakhmanov](#), [E. A. Popova](#)

The paper aims to study relation between the distributions of the young stellar objects (YSOs) of different ages and the gas-dust constituents of the S254-S258 star-formation complex. This is necessary to study the time evolution of the YSO distribution with respect to the gas and dust compounds which are responsible for the birth of the young stars. For this purpose we use correlation analysis between different gas, dust and YSOs tracers. We compared the large-scale CO, HCO<sup>+</sup>, near-IR extinction, and far-IR *Herschel* maps with the density of YSOs of the different evolutionary Classes. The direct correlation analysis between these maps was used together with the wavelet-based spatial correlation analysis. This analysis reveals a much tighter correlation of the gas-dust tracers with the distribution of Class I YSOs than with that of Class II YSOs. We argue that Class I YSOs which were initially born in the central bright cluster S255-IR (both N and S parts) during their evolution to Class II stage (~2 Myr) had enough time to travel through the whole S254-S258 star-formation region. Given that the region contains several isolated YSO clusters, the evolutionary link between these clusters and the bright central S255-IR (N and S) cluster can be considered. Despite the complexity of the YSO cluster formation in the non-uniform medium, the clusters of Class II YSOs in the S254-258 star-formation region can contain objects born in the different locations of the complex.

## 18. SiO Outflows as Tracers of Massive Star Formation in Infrared Dark Clouds

[Mengyao Liu](#), [Jonathan C. Tan](#), [Joshua Marvil](#), [Shuo Kong](#), [Viviana Rosero](#), [Paola Caselli](#), [Giuliana Cosentino](#)

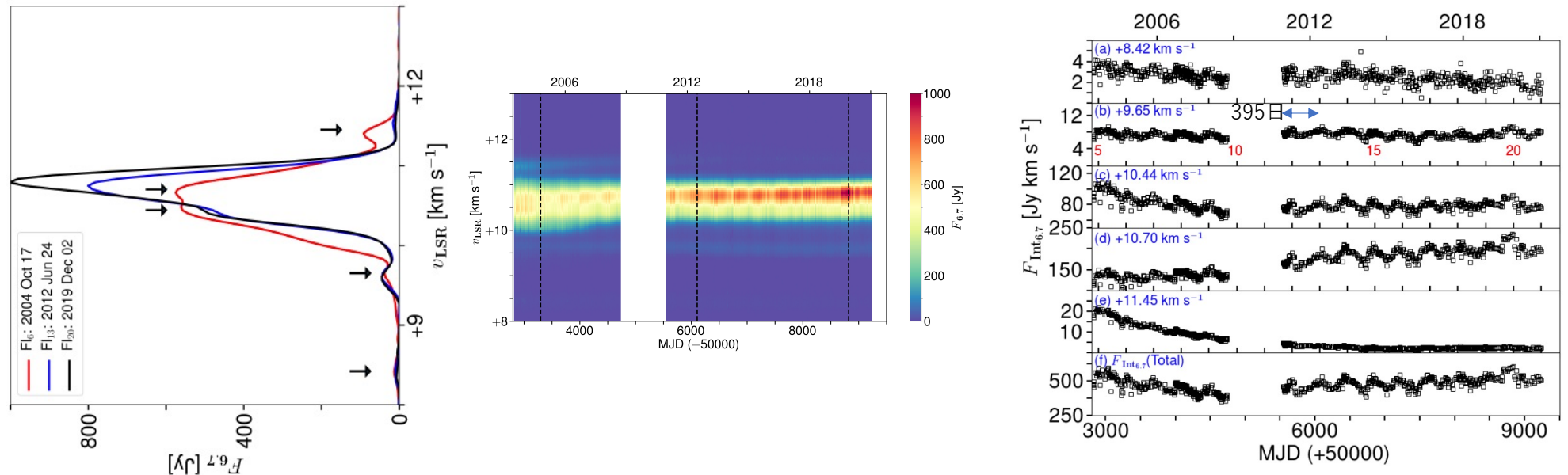
To study the early phases of massive star formation, we present ALMA observations of SiO(5-4) emission and VLA observations of 6 cm continuum emission towards 32 Infrared Dark Cloud (IRDC) clumps, spatially resolved down to  $\approx 0.05$  pc. Out of the 32 clumps, we detect SiO emission in 20 clumps, and in 11 of them the SiO emission is relatively strong and likely tracing protostellar outflows. Some SiO outflows are collimated, while others are less ordered. For the six strongest SiO outflows, we estimate basic outflow properties. In our entire sample, where there is SiO emission, we find 1.3 mm continuum and infrared emission nearby, but not vice versa. We build the spectral energy distributions (SEDs) of cores with 1.3 mm continuum emission and fit them with radiative transfer (RT) models. The low luminosities and stellar masses returned by SED fitting suggest these are early stage protostars. We see a slight trend of increasing SiO line luminosity with bolometric luminosity, which suggests more powerful shocks in the vicinity of more massive YSOs. We do not see a clear relation between the SiO luminosity and the evolutionary stage indicated by L/M. We conclude that as a protostar approaches a bolometric luminosity of  $\sim 10^2 L_{\odot}$ , the shocks in the outflow are generally strong enough to form SiO emission. The VLA 6 cm observations toward the 15 clumps with the strongest SiO emission detect emission in four clumps, which is likely shock ionized jets associated with the more massive ones of these protostellar cores.



## 19: Massive Protocluster of a Periodic Maser Source G188.95+0.89

[M. M. Mutie](#), [J. O. Chibueze](#), [K. El Bouchefry](#), [G. C. MacLeod](#), [J. Morgan](#), [P. Baki](#)

We report the results of ongoing monitoring of the 6.7 GHz CH<sub>3</sub>OH masers associated with G188.95+0.89. In these observations five features are periodically varying and at least two exhibit evidence of velocity drifts. It is not clear the cause of these velocity drifts. The spectra have varied significantly since detection in 1991. The 11.45 km s<sup>-1</sup> feature has decreased exponentially from 2003. Complementary ALMA 1.3 mm continuum and line observational results are also presented. Eight continuum cores (MM1 - MM8) were detected in G188.95+0.89. We derived the masses of the detected cores. G188.95+0.89 MM2 was resolved into 2 continuum cores (separated by 0.1 arcsec) in ALMA band 7 observations. Also CH<sub>3</sub>OH (4(2,2)-3(1,2)) thermal emission associated with MM2 is double peaked. We propose the presence of multiple (at least binary) young stellar objects in MM2. SiO emission exhibit a bow-shock morphology in MM2 while strong emission of <sup>12</sup>CO at the east and west of MM2 suggest the presence of an east-west bipolar outflow.



## 20: Proper motions of spectrally selected structures in the HH 83 outflow

[T.A. Movsessian](#), [T.Yu. Magakian](#), [A.V. Moiseev](#)

We continue our program of investigation of the proper motions of spectrally separated structures in the Herbig-Haro outflows with the aid of Fabry-Perot scanning interferometry. This work mainly focuses on the physical nature of various structures in the jets. The aim of the present study is to measure the proper motions of the previously discovered kinematically separated structures in the working surface of the HH 83 collimated outflow. We used observations from two epochs separated by 15 years, which were performed on the 6m telescope with Fabry-Perot scanning interferometer. We obtained images corresponding to different radial velocities for the two separate epochs, and used them to measure proper motions. In the course of our data analysis, we discovered a counter bow-shock of HH 83 flow with positive radial velocity, which makes this flow a relatively symmetric bipolar system. The second epoch observations confirm that the working surface of the flow is split into two structures with an exceptionally large ( $250 \text{ km s}^{-1}$ ) difference in radial velocity. The proper motions of these structures are almost equal, which suggests that they are physically connected. The asymmetry of the bow shock and the turning of proper motion vectors suggests a collision between the outflow and a dense cloud. The profile of the  $H\alpha$  line for the directly invisible infrared source HH 83 IRS, obtained by integration of the data within the reflection nebula, suggests it to be of P Cyg type with a broad absorption component characteristic of the FU Ori like objects. If this object underwent an FU Ori type outburst, which created the HH 83 working surfaces, its eruption took place about 1500 years ago according to the kinematical age of the outflow.